

Phase space mass bound for fermionic dark matter from dwarf spheroidal galaxies

Chiara Di Paolo,^{1*} Fabrizio Nesti,^{2,3,4,5†} and Francesco L. Villante^{5,6‡}

¹*SISSA/ISAS, Via Bonomea 265, 34136 Trieste, Italy*

²*Dipartimento di Fisica, Theoretical section, Università di Trieste, Strada Costiera 11, I-34151 Trieste, Italy*

³*Ruder Bošković Institute, Division of Theoretical Physics, Bijenička cesta 54, 10000, Zagreb, Croatia*

⁴*INFN Sez. Trieste, Via A. Valerio 2, 34127 Trieste, Italy*

⁵*Dipartimento di Scienze Fisiche e Chimiche, Università dell'Aquila, via Vetoio SNC, I-67100, L'Aquila, Italy*

⁶*INFN-LNGS, Via G. Acitelli 22, 67100, Assergi (L'Aquila), Italy*

19 January 2018

ABSTRACT

We reconsider the lower bound on the mass of a fermionic dark matter (DM) candidate resulting from the existence of known small Dwarf Spheroidal galaxies, in the hypothesis that their DM halo is constituted by degenerate fermions, with phase-space density limited by the Pauli exclusion principle. By relaxing the common assumption that the DM halo scale radius is tied to that of the luminous stellar component and by marginalizing on the unknown stellar velocity dispersion anisotropy, we prove that observations lead to rather weak constraints on the DM mass, that could be as low as tens of eV. In this scenario, however, the DM halos would be quite large and massive, so that a bound stems from the requirement that the time of orbital decay due to dynamical friction in the hosting Milky Way DM halo is longer than their lifetime. The smallest and nearest satellites Segue I and Willman I lead to a final lower bound of $m \gtrsim 100$ eV, still weaker than previous estimates but robust and independent on the model of DM formation and decoupling. We thus show that phase space constraints do not rule out the possibility of sub-keV fermionic DM.

to Giulia D.S.

Key words: dark matter – galaxies: dwarf – elementary particles – neutrinos

1 INTRODUCTION

Dark matter (DM) is believed to be a main actor in cosmology, to constitute the great majority of the mass in the universe and to rule the processes of structure formation. The so-called Λ CDM paradigm, in which one assumes a cold dark matter (CDM) candidate that decouples from the primordial plasma when non-relativistic, successfully reproduces the structure of the cosmos down to scales ~ 50 kpc.

A number of serious challenges to the Λ CDM paradigm have emerged on the scale of individual galaxies and their central structure, see e.g. Weinberg et al. (2014) for a recent review. For instance, collisionless N-body simulations predict that the DM density profile of virialized objects has a negative logarithmic slope towards the center (Flores & Primack 1994; Navarro et al. 1996b, 1997; Moore 1994; Moore

et al. 1999a). Such a ‘cuspy’ distribution is not well supported by observational data of rotation curves of spiral galaxies, which are better described by halos featuring a constant density core (Salucci & Burkert 2000). Moreover, the number of DM subhaloes expected according to Λ CDM paradigm is much larger than the observed number of satellite galaxies in the Milky Way (Moore et al. 1999b; Klypin et al. 1999), even accounting for the many recently discovered faint systems. It is still unclear whether the above problems require major changes to the Λ CDM paradigm. Models have been presented in which shallow DM cores arise naturally in a Λ CDM cosmology as a results of SN feedback or dynamical friction (Navarro et al. 1996a; Governato et al. 2010, 2012; Pontzen & Governato 2012). Alternative DM candidates, however, have to be considered with utmost attention.

The hypothesis of warm dark matter (WDM) decoupling from the plasma when mildly relativistic, has been advocated as a solution of the possible CDM issues. WDM in-

* chiara.dipaolo@sissa.it

† fabrizio.nesti@irb.hr

‡ francesco.villante@aquila.infn.it

roduces a non vanishing free streaming length below which structure formation is suppressed, giving rise to the correct abundance of substructures at small scales (Colin et al. 2000; Bode et al. 2001; Avila-Reese et al. 2001). Moreover, if we consider a generic fermionic dark matter (FDM) candidate, like the typical massive \sim keV warm sterile neutrino, the limit on the phase space density provided by the Pauli exclusion principle implies that DM has a minimal velocity dispersion and, thus, resists compression. As a consequence, FDM halos naturally produce a cored density profile whose radius R_h (for a fixed halo mass M_h) is a decreasing function of the mass m of the DM candidate, see next section for details. Being the most DM dominated astrophysical objects, dwarf spheroidal galaxies are the optimal candidates to test this scenario.

The possibility to constrain the DM particle mass by determining the DM phase space distribution was first considered in the seminal work by Tremaine & Gunn (1979). In the hypothesis of non-dissipative evolution, i.e. conservation of the maximal phase space density, it is possible to set a strong bounds on the DM mass $m > 300\text{--}700$ eV, see e.g. Dalcanton & Hogan (2001). These bounds stem from the primordial limit of the DM phase space density, and are not necessarily related to the fermionic nature of dark matter; indeed they apply also if dark matter can be treated as a collisionless gas collapsed via violent relaxation *à la* Lynden-Bell. However, they require the knowledge of the initial DM phase space density (and, thus, of the DM production mechanism) and the assumption that baryonic feedback cannot alter the maximum of the DM distribution function. A more general situation was studied by Gerhard & Spergel (1992) that pointed out the importance of constraints by dynamical friction on dwarf spheroidal galaxies in the Milky Way host halo, that as we will show still play the most important role.

Subsequent analyses (Bilic et al. 2001; Chavanis 2002; de Vega et al. 2014) modeled truly fermionic DM cores for instance by using a Thomas-Fermi self-gravitating-gas approach, suggesting that dwarf spheroidal galaxies host degenerate fermionic halos while larger and less dense galaxies behave as non-degenerate classical systems. Observational data on DSph galaxies were used in Boyarsky et al. (2009) to derive bounds of the order of 400 eV. Finally, in a recent analysis (Domcke & Urbano 2015) it was claimed that the rotation curves of the eight classical dwarf spheroidal galaxies of the Milky Way are well fitted by assuming DM cores composed by fully degenerate fermions with masses $m \simeq 200$ eV and allowing for a non vanishing anisotropy of the stellar component.

The observation that kinematic properties of dwarf spheroidal galaxies may be connected, in a relatively simple model, to the elementary properties of the DM candidate is extremely interesting. However, there is at the moment no evidence in favour of degenerate galactic cores. If all the smallest galactic cores were to be degenerate, their masses and radii should follow a relationship $M_h \propto R_h^{-3}$, as expected for degenerate fermionic systems and univocally determined by the mass m of the DM candidate. This behaviour in the plane (R_h, M_h) is presently not observed; on the contrary, the observation that the estimated

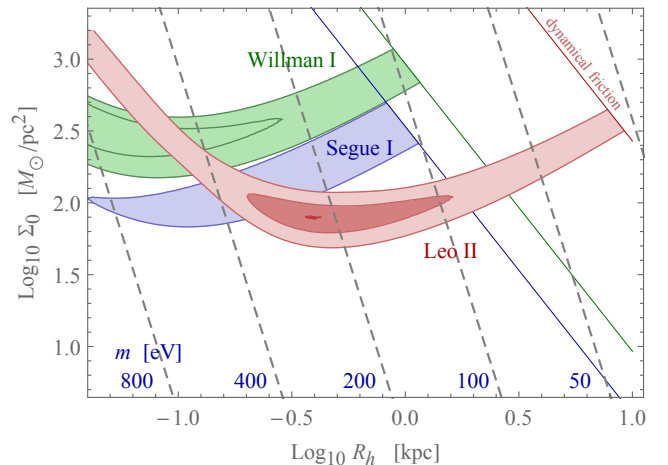


Figure 1. Plane $R_h - \Sigma_0$, describing the DM core. The shaded contours show the values of DM core sizes allowed for Willman I, Segue I and Leo II at 68% C.L. by the LOS velocities, and respecting the bound from the dynamical friction time.

surface densities of diverse kinds of galaxies is approximately constant (Donato et al. 2009; Salucci et al. 2012), $\Sigma_0 \sim M_h/R_h^2 \sim 100 M_\odot/\text{pc}^2$, can only be supported by non degenerate cores, because this relation lies almost orthogonal to the above degeneracy lines. Still, this argument cannot be used to rule out the existence of degenerate cores, because they could be present just in the smallest galaxies. These have a larger density, and therefore are candidate to support or exclude the hypothesis of fermionic DM with low mass.¹

In this paper we take a conservative attitude and determine a robust lower limit on the mass m of a fermionic DM particle from the properties of these smallest observed galaxies. We consider Willman I (Willman et al. 2011) and Segue I (Simon et al. 2011), which are among the smallest structures for which stellar velocity measurements are available, and the “classical” dwarf spheroidal Leo II from which restrictive bounds on m were obtained by Boyarsky et al. (2009) and Domcke & Urbano (2015). We determine bounds on the core radius R_h , mass M_h or surface density Σ_0 of the selected galaxies by performing a fit to the stellar line-of-sight velocity dispersion profile. The theoretical predictions are obtained through a standard Jeans analysis, including the role of the unknown velocity dispersion anisotropy of the stellar component. Moreover, we refrain from assuming that luminous matter traces the DM distribution, unlike many of the recent works, and thus leave as a free parameter the DM core radius.

We show in detail how, unless the anisotropy of stellar component will be constrained independently, the observed stellar velocity dispersion profiles lead to very poor constraints on the DM halo, and the possibility of very large \sim kpc halos cannot be ruled out. However, such large halos

¹ It is of course also possible that the evolution of structures is such that DM, although fermionic, never forms degenerate cores; in this situation it is still or even more important to assess the values of the DM mass that allows the realization of this scenario.

are at odds with their lifetime due to the dynamical friction within the Milky-Way (Binney & Tremaine 2008). This provides a further quantitative limit on the DM halo size, allowing us to finally constrain the DM particle mass m . To facilitate the reader, our results are anticipated in Figure 1 that contains a synthesis of our work before discussing the technical details.

The final limit that we obtain, $m \gtrsim 100$ eV, is less restrictive but more solid than previously quoted bounds (Boyarsky et al. 2009; Domcke & Urbano 2015) which rely on the assumption that the DM core radius is equal to the half-light radius, or analogously that the escape velocity from the DM core is determined by the stellar velocity dispersion. Moreover, our limit is fairly model-independent because it is based only on the present phase-space density of DM particles and does not require any assumption on their initial distribution or their evolution (see e.g. Boyarsky et al. (2009) for a discussion of the model-dependent bounds that can be obtained for a dissipationless DM candidate by considering specific production mechanisms). Restrictive limits ($m \gtrsim$ few keV) on sterile neutrino mass can be also obtained from the analysis of the Ly- α forest data, see e.g. Iršič et al. (2017) for a recent update. It should be noted, however, that this analysis is not directly sensitive to DM particle mass, as Ly- α data essentially probe the power spectrum of density fluctuations at comoving scales \sim Mpc, by constraining the DM free streaming length. Since this quantity can be related to the particle mass only within a specific DM model, the Ly- α bound cannot be applied to a generic fermionic candidate, unlike from the limit derived in this paper.

The plan of the paper is the following: in section 2 we describe the physics relevant for degenerate fermionic dark matter halos, while in section 3 we lay down the possible strategies to constrain the mass of the dark matter candidate from the observational data. In section 4 we describe the results for the Leo II, Willman I and Segue I dwarf galaxies, by paying also attention to the possibility that some of these galaxies are instead non-degenerate. We present also a consistent estimate for the ensuing bound on the DM mass in the case of the other known dsph galaxies. In section 5 we summarize the conclusions and possible outlook. Finally, for convenience we briefly review in Appendix A the technicalities relative to degenerate fermionic halos, as well as the Thomas-Fermi analysis for non exactly degenerate ones.

2 THE FDM HYPOTHESIS

We consider the equilibrium configuration for an ensemble of self-gravitating DM fermions of mass m and g internal (spin) degrees of freedom. The assumption of fermionic particles implies the upper limit for the DM phase space distribution function that, as reviewed in appendix A, translates into a lower limit for the DM velocity dispersion

$$\begin{aligned} \sigma_{\text{DM}}^2 &\geq \sigma_{\text{DM,min}}^2(\rho) = \frac{1}{5} \left(\frac{6 \pi^2 \hbar^3 \rho}{g m^4} \right)^{2/3} \\ &= 7.56 \left(\frac{\text{km}}{\text{s}} \right)^2 \left(\frac{g}{2} \right)^{-2/3} \left(\frac{m}{1 \text{ keV}} \right)^{-8/3} \left(\frac{\rho}{\text{M}_\odot/\text{pc}^3} \right)^{2/3} \end{aligned} \quad (1)$$

as a function of the mass density ρ of the system. This bound becomes effective and very stringent in the regions of high density. As a consequence, fermionic DM halos resist compression and cannot have arbitrary size.

The strong degeneracy limit, in which the velocity dispersion is assumed to have the minimal value $\sigma_{\text{DM,min}}^2(\rho)$, represents the most compact configuration for a self-gravitating fermionic halo. The density profiles of such fully degenerate halos are universal. They depend only on one free parameter and can be expressed (apart from a normalization factor and a scale radius which are related, see the following) in terms of the solution of the well-known Lane-Emden equation, see equation (A13). As shown in the appendix, for our purposes the degenerate profiles are very well approximated by the function:

$$\rho(r) = \rho_0 \cos^3 \left[\frac{25}{88} \pi x \right], \quad x = r/R_h, \quad (2)$$

where ρ_0 is the central DM halo density. The halo radius R_h is defined by the condition

$$\rho(R_h) = \rho_0/4 \quad (3)$$

and is related to the central density ρ_0 and to the properties of the DM particle by the numerical relation

$$R_h = 42.4 \text{ pc} \left(\frac{g}{2} \right)^{-1/3} \left(\frac{m}{1 \text{ keV}} \right)^{-4/3} \left(\frac{\rho_0}{\text{M}_\odot/\text{pc}^3} \right)^{-1/6}. \quad (4)$$

This value represents also the minimal admissible radius for a fermionic structure since for smaller radii the gravitational potential $\phi \sim -G \rho_0 R_h^2$ is lower (in modulus) than $\sigma_{\text{DM,min}}^2 \sim (\rho_0/g)^{2/3} m^{-8/3}$ and the system is not stable.

Larger non degenerate structures are admissible because they can have $\sigma_{\text{DM}}^2 \geq \sigma_{\text{DM,min}}^2$ that prevents gravitational collapse. Unlike in the completely degenerate case, their properties cannot be univocally predicted because the velocity dispersion is not determined by the mass density and not directly linked to the DM particle properties. Isothermal halos with arbitrary level of degeneration can be studied by using the Thomas-Fermi approach as reviewed in Appendix A. Interestingly, it is found that when R_h is just 2–3 times larger than the minimal value (4), the fermionic nature of DM particles can be neglected, i.e. the resulting structures are essentially indistinguishable from isothermal halos obtained by assuming classical Maxwell-Boltzmann statistics and arbitrary large values of the particle mass m .

For fully degenerate fermionic structures, by using equation (4) one can predict their surface density $\Sigma_0 \equiv \rho_0 R_h$

$$\frac{\Sigma_0}{\text{M}_\odot/\text{pc}^2} = 0.584 \left(\frac{g}{2} \right)^{-2} \left(\frac{m}{1 \text{ keV}} \right)^{-8} \left(\frac{R_h}{100 \text{ pc}} \right)^{-5} \quad (5)$$

as well as their mass M_h , defined as the mass enclosed within the radius R_h :

$$\frac{M_h}{10^7 \text{ M}_\odot} = 1.18 \left(\frac{g}{2} \right)^{-1/3} \left(\frac{m}{1 \text{ keV}} \right)^{-8} \left(\frac{R_h}{10 \text{ pc}} \right)^{-3}. \quad (6)$$

The radius, surface density and mass of degenerate halos are not independent quantities, being $M_h \simeq 2.02 \rho_0 R_h^3 = 2.02 \Sigma_0 R_h^2$ for the density profile (2). For definiteness, we perform our analysis in the plane (R_h, Σ_0) but equivalent

bounds are clearly obtained by using any couples of the three quantities R_h , Σ_0 and M_h .

In Figure 1 we have reported as gray dashed lines in the plane (R_h, Σ_0) the points relative to fully degenerate systems for selected values of the DM particle mass m and assuming $g = 2$. Eqs. (5) and (6) define the lower limits for surface densities and masses of fermionic DM halos. The regions to the left of the gray lines in the plane (R_h, Σ_0) , are not compatible with the assumption that the halo is composed by fermionic particles. Note that for fixed surface density, the smaller is the particle mass the larger has to be the core radius. As a consequence, the observational determinations of halo radii R_h and surface densities Σ_0 can be translated into lower limits for the mass m of fermionic dark matter candidates:

$$\frac{m}{\text{keV}} \geq 0.53 \left(\frac{g}{2}\right)^{-1/4} \left(\frac{\Sigma_0}{100 M_\odot/\text{pc}^2}\right)^{-1/8} \left(\frac{R_h}{100 \text{ pc}}\right)^{-5/8} \quad (7)$$

and we note the reduced dependence on Σ_0 .

If galactic cores were to be commonly degenerate, one should arguably observe a clustering along the lines defined by equation (5) in the plane (R_h, Σ_0) , at least for the smallest structures. This clustering is presently not observed. Instead, the estimated surface densities of diverse kinds of observed galaxies appear to be approximately constant (Donato et al. 2009; Salucci et al. 2012), $\Sigma_0 \sim 100 M_\odot/\text{pc}^2$, a fact that can only be supported by non degenerate cores, because this relation lies almost orthogonal to the degeneracy lines.

This argument cannot be used to rule out the fermionic nature of DM, or the occurrence of degenerate halos, because even if all large galaxies host a non-degenerate DM halo, degenerate cores could be present in the smallest objects, of limited number and maybe even too small to be observed. Therefore, what one can do at present is to obtain a lower limit on the mass of a fermionic DM candidate from the existence of the smallest galaxies, once their properties (radius, mass and/or surface density) are determined. It is our aim to reassess in this way the present bound on m .

3 STRATEGIES

The standard mass estimation methods applied to dwarf spheroidal galaxies, like those described in Wolf et al. (2010), are not sufficient for our purposes. In fact, they provide an estimator of the mass $M_{1/2}$ enclosed inside the half-light radius $R_{1/2}$, but this radius is not necessarily representative of the DM distribution and might be in principle (much) smaller than the halo size R_h . In other words, the quantity $M_{1/2}$ represents only a lower limit on the core mass M_h but does not provide an upper constraint.

In e.g. Boyarsky et al. (2009) and Domcke & Urbano (2015), lower bounds on the mass of FDM candidates were obtained by assuming that $R_h \simeq R_{1/2}$, i.e. $M_h \simeq M_{1/2}$ and/or by assuming that the stellar velocity dispersion can be used to estimate the escape velocity from the DM core. This is only allowed if we assume that luminous matter

traces DM distribution. However, this assumption may well be violated, especially in the considered scenario in which the properties of the DM distribution are not only determined by gravitational interactions but also by the fermionic nature of DM. One may also recall that for larger galaxies, like the Milky Way or elliptical galaxies, the scale lengths of stellar and dark components can differ greatly, with the dark component extending typically some factors more than the stellar one.

Along these arguments, in this work we proceed in more generality, treating R_h and M_h as independent properties of the DM halo. We only use $R_{1/2}$ and $M_{1/2}$ in a preliminary stage to select, by using the values tabulated in Wolf et al. (2010) and equation (6), the dwarf spheroidal galaxies Willman I (Willman et al. 2011) and Segue I (Simon et al. 2011) as the most promising candidates for constraining m . In addition to these two galaxies, which are among the smallest structures for which stellar velocity measurements are available, we also consider the ‘‘classical’’ dwarf spheroidal Leo II from which restrictive bounds on m were obtained by Boyarsky et al. (2009) and Domcke & Urbano (2015).

For each galaxy, we determine the DM halo properties, core radius and mass (or surface density) by performing a fit of the stellar line-of-sight velocity dispersion profile as predicted by the model through the Jeans analysis, to the observed data. We also consider the role of the possible stellar velocity dispersion anisotropy. As was already suggested in the past (see e.g. Walker (2013)) in most cases the poor data and the unknown anisotropy lead to very poor constraints on the DM halo, and the possibility of very large $\sim\text{kpc}$ halo can not be ruled out. We then consider that such large haloes would be associated with unphysically short orbital lifetimes due to the dynamical friction within the Milky-Way. This fact provides a further quantitative constraint on the DM halo size, and thus allows us to constrain the DM particle mass m .

3.1 Spherical Jeans analysis

Assuming that the stellar component is virialized within the gravitational potential dominated by the DM component, the standard spherical Jeans equation

$$\left(\frac{\partial}{\partial r} + \frac{2\beta}{r}\right)(n_*\sigma_r^2) = -n_*\frac{GM(r)}{r^2} \quad (8)$$

allows one to relate the velocity dispersion profile of stars to the DM mass distribution $M(r)$. In the above, G is the Newton constant, $n_*(r)$ is the stellar number density, σ_r^2 is the radial velocity dispersion of stars, and $\beta \equiv 1 - \sigma_\perp^2/\sigma_r^2$ is its anisotropy, which in principle can depend on radius. We first discuss the case of zero anisotropy, and later comment on its role. Our final results are obtained by treating β as a nuisance parameter. A number of other aspects, like the possible coexistence of more than one stellar component, or non-complete virialization, are further factors of uncertainty that may not be easily removed.

We model the density profile of the stellar component for each dwarf spheroidal galaxy by means of a Plummer

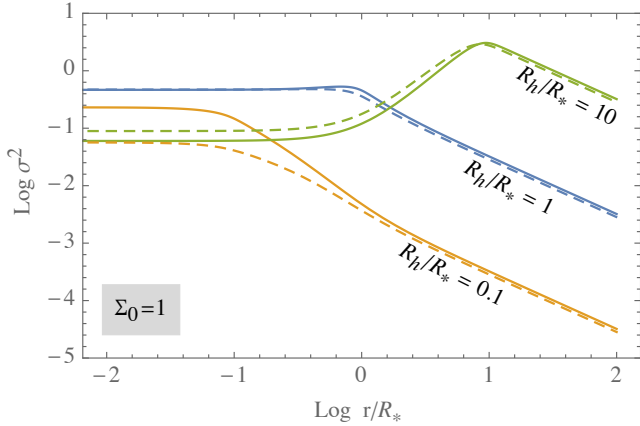


Figure 2. Stellar velocity dispersion profiles (solid) for representative DM core radii and $\beta = 0$. The dashed curves show the line-of-sight projected dispersion velocity profiles.

density profile with specific scale radius R_* :

$$n_*(r) = n_0 (1 + x^2)^{-5/2}, \quad x = r/R_*, \quad (9)$$

and the central density n_0 plays no role in the following. Clearly, the applicability of this density profile to real and poorly known galaxies is an other element of uncertainty.

Equation (8) can be integrated in favor of σ_r^2 , once the dark matter mass distribution $M(r)$ is determined by the DM density equation (2). The resulting stellar velocity dispersion is shown in Figure 2, for three representative cases of R_h smaller, equal or larger than the stellar scale radius R_* . The profiles shown are illustrative and are obtained by normalizing to a fixed surface density $\Sigma_0 = \rho_0 R_h = 1$. In fact, once the radius R_h is fixed, the DM central density ρ_0 or the surface density Σ_0 represent just a multiplicative constant factor for the mass function $M(r)$ and do not affect the radial dependence of σ_r^2 .

We see from Figure 2 that if the DM halo is smaller than the Plummer radius, $R_h \leq R_*$, the stellar velocity dispersion starts to fall as soon as the DM density vanishes, reflecting the decrease of the gravitational potential. On the other hand if the DM distribution is more extended than the stellar one, $R_h \geq R_*$, the stellar velocity dispersion has to increase in the regions where the Plummer density drops. In few words, the slope of the stellar velocity dispersion $\partial \ln \sigma_r^2 / \partial \ln r$ is related to the characteristic sizes R_* and R_h of the galactic components and could, thus, be used to constrain the DM distribution.

In order to compare with observational data, one has also to consider that only the velocity dispersion *along the line of sight* (LOS) is measurable:

$$\sigma_{\text{los}}^2(R) = \frac{1}{\Sigma_*} \int_{R^2}^{\infty} dr^2 \frac{n_*(r)}{\sqrt{r^2 - R^2}} \sigma_r^2 \left[1 - \beta \frac{R^2}{r^2} \right], \quad (10)$$

where $\Sigma_*(R) = \int_{R^2}^{\infty} dr^2 n_*(r) / \sqrt{r^2 - R^2}$ is the projected stellar (surface) density. In Figure 2, we show with dashed lines the LOS velocity dispersion for the three cases described previously. They retain the same behaviour of σ_r^2 , showing that the observed LOS velocity dispersion profile

$\sigma_{\text{los}}^2(R)$ can in principle be used to constrain the size of the DM core.

3.2 Analysis for the smallest objects

In order to obtain the most restrictive bounds on the mass of the FDM particle, below we will consider Willman I (Willman et al. 2011) and Segue I (Simon et al. 2011) which are among the smallest observed galactic structures. The problem with these objects is that the number of stars for which a measure of velocity is available and which pass quality cuts is quite small (i.e. less than 50). As a consequence, it is not possible to determine the velocity dispersion in radial bins sufficiently localized to be compared directly with the profile in equation (10). One can still appreciate the characteristic signature of a large DM core, i.e. an increasing slope of the stellar dispersion velocity between $r \sim R_*$ and $r \sim R_h$, by determining the velocity dispersion in few relatively large bins with dimension $\Delta r \sim R_*$.

In order to perform such analysis, we define the *average* LOS velocity dispersion in a bin $r \in [R_1, R_2]$,

$$\overline{\sigma_{\text{los}}^2}(R_1, R_2) = \frac{1}{N_*(R_1, R_2)} \int_{R_1}^{R_2} dr 2\pi r \Sigma_*(r) \sigma_{\text{los}}^2(r), \quad (11)$$

where $N_*(R_1, R_2) = \int_{R_1}^{R_2} dr 2\pi r \Sigma_*(r)$ is the cumulative number of stars between two radii. Using (10), and assuming constant β , we find

$$\overline{\sigma_{\text{los}}^2} = \frac{1}{N_*(R_1, R_2)} \int_{R_1}^{\infty} dr 4\pi r^2 n_* \sigma_r^2 \mathcal{F}(r, \beta; R_1, R_2), \quad (12)$$

where the adimensional function $\mathcal{F}(r, \beta; R_1, R_2)$ is

$$\mathcal{F}(r, \beta; R_1, R_2) = \left\{ \left[\sqrt{r^2 - R_1^2} - \sqrt{r^2 - B^2} \right] \frac{(3 - 2\beta)}{3r} + \frac{\beta}{3r^3} \left[B^2 \sqrt{r^2 - B^2} - R_1^2 \sqrt{r^2 - R_1^2} \right] \right\} \quad (13)$$

with $B = \min\{r, R_2\}$.²

For illustrative purposes, we show in Figure 3 as solid lines the behaviour of the average LOS velocity dispersion calculated in two bins $[0, R_*]$ and $[R_*, 3R_*]$ as a function of the DM core radius R_h , for $\beta = 0$. One can observe that the average LOS dispersion velocity in the external bin overshoots the internal one as soon as $R_h/R_* \gtrsim 2$. This demonstrates that even with two single bins, and provided the uncertainties on the observed dispersion velocity are not too large, one could constrain the DM core size. For instance, if the observed dispersion velocities in two or more bins in the vicinity of $r \simeq R_*$ are approximately the same, one could rule out the possibility that DM extends much beyond the stellar component.

From the plot one can make also other remarks. Clearly, the more the DM core extends beyond the stellar component ($R_h/R_* > 1$) the less its actual density profile beyond R_h is relevant for the stellar physics, because the DM density is

² The number of stars in a bin $N_*(R_1, R_2)$ can be also calculated as $N_*(R_1, R_2) = \int_{R_1}^{\infty} dr 4\pi r^2 n_*(r) \mathcal{F}(r, \beta = 0; R_1, R_2)$.

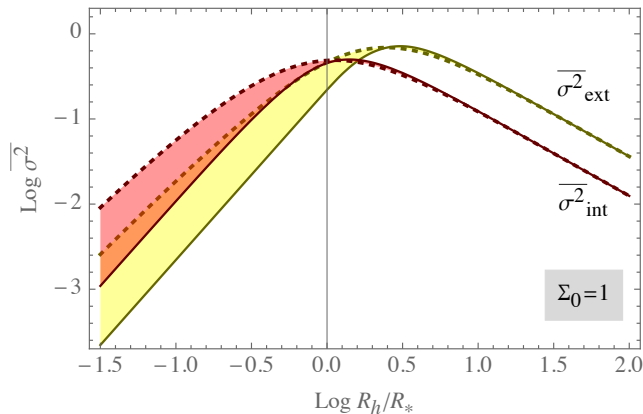


Figure 3. Averaged stellar velocity dispersion in two bins, taken here as *int* = $[0, r_*$] (red) and *ext* = $[r_*, 3r_*$] (yellow), for $\beta = 0$. The dashed curves show the same for a Burkert profile (non-degenerate fermions).

anyway constant in the region where the stars trace the gravitational potential. On the other hand, one can expect that if the DM core is smaller than the stellar scale ($R_h/R_* < 1$) the actual shape of the DM profile out of its core will influence the resulting stellar velocity dispersion. To show this effect, we have repeated the analysis for Burkert DM profiles, also reported in Figure 3 as dashed lines, which confirms the dependence on the profile shape for $R_h < R_*$. On the other hand, for $R_h > R_*$, the solid and dashed curves are overlapping, i.e. the predicted dispersion does not depend on the shape of the DM profile, making the analysis more robust.

Unfortunately, as we shall discuss for the specific cases of Segue I and Wilman I, the analysis outlined in this section is considerably hampered by the large uncertainties in each bin of the observed velocity dispersion. In addition, it is also severely limited by the unknown velocity anisotropy.

3.3 The role of anisotropy

As is well known and as we will see in detail, the unknown stellar velocity dispersion anisotropy β limits severely the possibility to extract the DM core radius R_h from observational data. Indeed, in the absence of direct information, the quantity β has to be treated as a nuisance parameter that has to be removed in order to compare a mass model with observations (see e.g. Walker et al. (2007) and Ullio & Valli (2016) for a recent critical discussion). The role of β can be understood by rewriting the Jeans equation (8) in the form

$$\frac{\partial \ln \sigma_r^2}{\partial \ln r} = -\frac{1}{\sigma_r^2} \frac{GM}{r} - \gamma_* - 2\beta \quad (14)$$

where $\gamma_* = d \ln n_*/d \ln r$ is the slope of the stellar number density, that runs from ~ 0 near the center to negative values out of R_* . Note that the first two terms in the r.h.s. which are related to DM and stellar distributions have opposite signs, being negative the first and positive the second. In the case of zero anisotropy, the slope of the velocity dispersion vanishes at the galactic center, i.e. $\partial \ln \sigma_r^2 / \partial \ln r = 0$ for $r = 0$, since these two terms are both equal to zero in the origin. If the

DM halo extends outside the stellar scale radius, the term γ_* starts to grow (in modulus) at $r \simeq R_*$ while $GM(r)/r\sigma_r^2$ is still negligible, and determines the positive slope of σ_r^2 observed in Figure 2. Whereas the observed stellar velocity dispersion does not feature such a growth at large distances, one can set an upper bound on the DM core radius, that can not be much larger than the stellar scale radius R_* .

The presence of a non vanishing anisotropy can clearly alter this scenario. In particular, a positive β can compensate the effect of γ_* reducing the outer slope of σ_r^2 , even in presence of a DM distribution extending well beyond the stellar radius. However, this effect is limited by the fact that the anisotropy parameter is limited to be less than 1. As a result, the case $\beta = 1$ leads to weaker upper bound on the core radius R_h , and basically the most conservative. The opposite holds for negative β values that can give quite small slope $\partial \ln \sigma_r^2 / \partial \ln r \geq 0$ even for mass models with $R_h \leq R_*$. Because a negative β is unconstrained, this limits the possibility of setting a lower bound on R_h in dwarf spheroidals and assessing the cusp-core problem at such short scales.

Note that, for the purpose of determining an upper limit for the core radius R_h , it is not even necessary to consider a generic $\beta(r)$ since the most relevant fact is the presence of the upper bound $\beta < 1$. In our analysis, we assume a constant anisotropy parameter β and we treat it as a nuisance parameter.

In order to do this, we adopt the following philosophy: for each set of DM core radius R_h and surface density Σ_0 we scan over the complete physically allowed range $-\infty \leq \beta \leq 1$, and if there exists a value of β that provides a good fit to the observational data, then the hypothesis of a degenerate core with those parameters cannot be rejected. Following a frequentist approach, the level of compatibility with data is assessed by defining a standard χ^2 function, see section 4.1. This is eventually minimized with respect to β . This procedure allows us to obtain the most conservative bounds.

The comprehensive range in β that we adopt, reflects our present ignorance of the dispersion anisotropy. Clearly, if in the future independent constraints on the anisotropy parameter will become available, this procedure might be improved.

It should be noted that an additional source of uncertainty is due to the slope of the density profile γ_* . As a general rule (see equation (14)) the role of γ_* in the outer regions is similar to that of β : the more negative γ_* is, the stronger is the rise in the external σ_r and thus the more restrictive the bound would be. The Plummer profile that we adopt reaches quite steep values (-5) of the slope in the outer region and thus can be taken as a reasonable benchmark. Because in practice the precise slope of the density profile is extremely hard to constrain from observations, especially for the smallest objects, this additional uncertainty should be kept in mind.

3.4 Dynamical friction

The mass of dwarf spheroidals can be limited from above because they are subject to dynamical friction in the Milky-

Way DM halo. Their orbit decay with a characteristic time scale that can be estimated from the Chandrasekhar's formula (Binney & Tremaine 2008)

$$t_{\text{fric}} = \frac{10^{10} \text{ y}}{\ln \Lambda} \left(\frac{D}{60 \text{ kpc}} \right)^2 \left(\frac{v}{220 \text{ km/s}} \right) \left(\frac{2 \cdot 10^{10} M_{\odot}}{M_h} \right) \quad (15)$$

where v is the velocity of the dwarf galaxy and D is its distance from the Milky-Way center. The Coulomb logarithm in the above equation is given by

$$\ln \Lambda = \ln \left(\frac{b_{\text{max}}}{b_{\text{min}}} \right), \quad (16)$$

where b_{max} and b_{min} are the maximum and minimum impact parameters. These can be estimated as (Binney & Tremaine 2008; Just et al. 2011):

$$b_{\text{max}} = - \left(\frac{d \ln \rho_{\text{MW}}}{dr} \right)^{-1} \simeq \frac{D}{\gamma}, \quad b_{\text{min}} = \max \left\{ R_h, \frac{GM_h}{v_{\text{typ}}^2} \right\}, \quad (17)$$

where v_{typ} is the virial velocity and we assumed that the Milky Way DM density scales approximately as $\rho_{\text{MW}} \propto D^{-\gamma}$ with $\gamma \simeq 2$ in the vicinity of the objects considered.³

Chandrasekhar's formula (15) is known to fail when the mass of the mass M_h of the satellite becomes comparable to the mass of the host system that lies interior to the satellite's orbit and/or the density of host system is constant, see e.g. Read et al. (2006). In the cases of our interest, however, none of these conditions apply and equation (15) provides a remarkably accurate description. By requiring $t_{\text{fric}} \gtrsim 10^{10} \text{ y}$, and by considering that the typical velocity of satellites should be of the order of the Galactic virial velocities at those distances $\sim 220 \text{ km/s}$ (Nesti & Salucci 2013), one finds a bound on the mass M_h that depends on the distance of the dwarf galaxy from the Galactic center.

Note that the existence of an upper limit for M_h does not imply by itself the possibility to constraints the FDM scenario. It was noted, however, in Gerhard & Spergel (1992) that if the DM density of dwarf spheroidal galaxies can be determined from velocity dispersion data, the upper bound on M_h can be used to obtain an upper limit on R_h , thus constraining the mass m of hypothetical FDM particles.

4 RESULTS

4.1 A small classical Dwarf - Leo II

As a paradigmatic case, we first analyze the case of Leo II, the smallest among the so-called 'classical' dwarf spheroidal satellite galaxies of the MW. The stellar number density of Leo II is well modeled by a Plummer profile with scale length $R_* = 177 \text{ pc}$. In Figure 4 we report the observed stellar LOS velocity dispersion, $\sigma_i^2 \pm \delta\sigma_i^2$, measured in 11 bins centered at the radii r_i . We compare these data with the LOS velocity dispersion predicted in (10) for the fully

³ For degenerate cores, the halo radius R_h defined in equation (A14) is sufficiently close to the half-mass radius of the DM distribution.

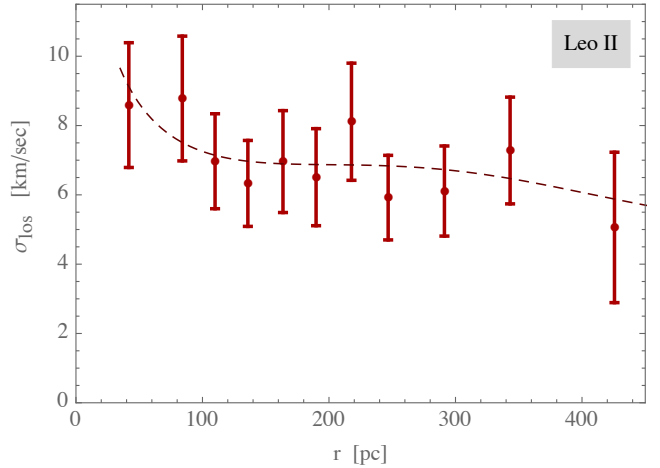


Figure 4. Stellar line-of-sight velocity dispersions for Leo II. The dashed line represents the best fit, achieved for $\beta = 0.6$.

degenerate fermionic DM halo, $\overline{\sigma}_i^2 \equiv \sigma_{\text{los}}^2(r_i)$, by defining a standard χ^2 test:

$$\chi^2(R_h, \Sigma_0, \beta) = \sum_{i \in \text{bins}} \left(\frac{\sigma_i^2 - \overline{\sigma}_i^2}{\delta\sigma_i^2} \right)^2. \quad (18)$$

The model parameters are the DM core radius R_h and surface density $\Sigma_0 \equiv \rho_0 R_h$, plus the anisotropy β .

Our results are shown in Figure 5. In the left frame, we plot the χ^2 contours in the plane (R_h, Σ_0) , corresponding to 68% CL exclusion for 11 degrees of freedom (dof), obtained by assuming fixed values of $\beta = -0.5, \dots, 1$. In the right frame, we eliminate the nuisance parameter β . As discussed in sec. 3.3, we use a conservative approach that does not require the introduction of a prior on the anisotropy distribution. Namely, for fixed model parameters R_h and Σ_0 , we minimize the χ^2 over the admissible range $-\infty \leq \beta \leq 1$; we then compare the minimal value with a χ^2 probability distribution with $11 - 1 = 10$ dof to possibly reject the assumed parameters. The light shaded area in the right frame of Figure 5 corresponds to $\chi^2 = 11.5$ that gives 68% CL exclusion.⁴

The best fit model (which has $\chi_{\text{bf}}^2 \simeq 2.5$) is obtained with $\beta = 0.6$ and is relative to a core size $R_h \simeq 400 \text{ pc}$ and surface density $\Sigma_0 \simeq 75 M_{\odot}/\text{pc}^2$. It provides a very good fit to the observational data, as it is shown by the velocity dispersion profile in figure 4. Being this a fully degenerate halo, the couple of parameters (R_h, Σ_0) corresponds to a well defined mass m of the FDM candidate, which for the best fit corresponds to $m \simeq 0.23 \text{ keV}$, in good agreement with the value suggested by Domcke & Urbano (2015).

On the other hand, a non degenerate fermionic core can

⁴ Because we are interested in a bound on m by excluding a region of the (R_h, Σ_0) plane, we use the absolute χ^2 to determine the level of compatibility with observational data. If instead one assumes that the FDM hypothesis is correct, the 68% CL allowed region in the plane is determined by $\Delta\chi^2 \equiv \chi^2 - \chi_{\text{bf}}^2 = 2.3$ (for 2 dof). For completeness, we show this region with dark shaded area in Figure 5.

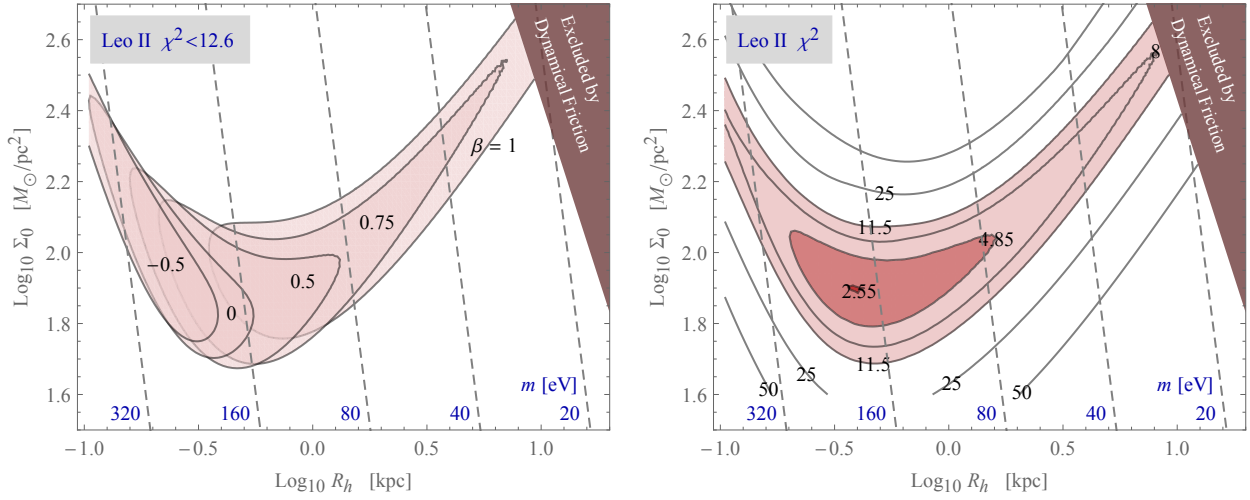


Figure 5. LEO II – Left: Contours of compatibility with data at 68% probability ($\chi^2 \lesssim 12.6$, for 11 dof) as a function of the degenerate DM core parameters, for various values of the dispersion anisotropy β . Right: Contours of best χ^2 in the plane (R_h, σ_0) after eliminating the anisotropy β . The light shaded region is compatible with the observational data at 68% CL ($\chi^2 \lesssim 11.5$, for 11-1=10 dof). The darker shading shows the region preferred by data at 68% CL ($\Delta\chi^2 = 2.3$), if one *assumes* the FDM hypothesis as true.

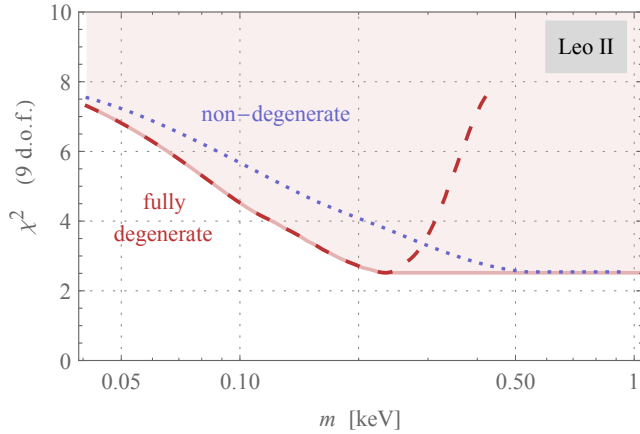


Figure 6. LeoII - The χ^2 as a function of the particle mass m with different assumptions for the DM distribution. The red dashed line is obtained, after minimization with respect to Σ_0 and β , for fully degenerate cores with radius $R_h = R_{h,\min}(m, \Sigma_0)$. The blue dotted line is similarly obtained for a non-degenerate cored (Burkert) profile with radius $R_h = 2 R_{h,\min}(m, \Sigma_0)$. The light-red solid line and the shaded region represents the overall minimal $\chi^2(m)$, obtained by considering that DM cores with generic radii $R_h \geq R_{h,\min}(m, \Sigma_0)$ are allowed for a fermionic DM candidate.

have generic radii R_h larger than the minimal (degenerate) value as found from equation (5)

$$R_{h,\min} = 90 \text{ pc} \left(\frac{g}{2}\right)^{-2/5} \left(\frac{m}{1 \text{ keV}}\right)^{-8/5} \left(\frac{\Sigma_0}{M_\odot \text{ pc}^{-3}}\right)^{-1/5} \quad (19)$$

which is shown as gray dashed lines in figure 5 for selected values m . By using the inequality $R_{h,\min} \leq R_h$, one would like to obtain a lower bound on the DM particle mass directly from the constraints on the halo parameters R_h and

Σ_0 , as in equation (7). However, one can see that unless the anisotropy β is constrained independently, velocity dispersion data do not allow to set limits on m . In particular, for maximal values of $\beta \sim 1$, i.e. radial motion of stars, very small values of m are allowed by the data and are relative to multi-kpc halos, as it seen in figure 5. This situation is most likely not realistic, being unplausible that such a huge DM halo host a stellar system of just few hundredths pc and small velocity dispersion. It is however not possible to give at this stage a quantitative support to this comment, using dispersion data alone. Indeed, in the upper-right part of the plots, the χ^2 becomes flattish for $R_h \gg R_*$ because the limited extent of the stellar component does not permit to constrain a much larger DM halo.

The above conclusion can be made more quantitative by producing a one-dimensional χ^2 profile as a function of m . This is shown in Figure 6 which is built as follows.

First, we obtain the red dashed curve, relative to fully degenerate models, by expressing the core radius ($R_h = R_{h,\min}$) as a function of the mass m through equation (19), and then minimizing the χ^2 with respect to Σ_0 , in addition to β . From this curve one finds directly that no lower limit on the particle mass m can be obtained, even at 68% CL that would require $\chi^2 > 10.4$ (for 11 - 2 = 9 dof). The curve also becomes flattish for $m \lesssim 50 \text{ eV}$, corresponding to the fact that for small masses the DM core becomes much larger than the stellar component, whose properties can only probe the central density of the DM distribution, but not its extension. Incidentally, this also means that the stellar velocity dispersion can be equally fitted by non-degenerate cored DM profiles with the same central density, the outer profile being irrelevant.

Then, on the rising part of the red dashed curve, towards large values of m , we note that while the fit worsens progressively as the degenerate core shrinks, one can not set an upper bound on m , because the size of a degenerate core

is just a lower limit, and any good fit with a given radius can also be produced with higher m as a non-degenerate configuration. Indeed, the mass m has to play no role in the non-degenerate regime. Thus, the final χ^2 has to be thought as independent from the DM mass, i.e. flat, starting just beyond the minimum of the degenerate case. This is depicted as a light-red solid line and by the shaded region in Figure 6.

This argument is confirmed by repeating the whole analysis with a non-degenerate cored density profile (we adopt the Burkert density profile taking a core radius 2 times larger than the minimal value, $R_h = 2R_{h,\min}$, see appendix A). This gives the blue dotted curve in Figure 6. As expected, the non-degenerate profile leads to better fits for large masses while the χ^2 slowly converges to the degenerate case at the left end of the plot. This test could be repeated by considering other admissible non-degenerate profiles, and/or different $R_h > R_{h,\min}$, and the envelope of the relative curves will produce the overall minimal χ^2 as depicted as the red solid line.

Even if stellar velocity dispersion data, taken alone, do not allow to obtain a limit on m , the mass of the DM particle can be constrained by considering that the halo decay time due to dynamical friction (15) becomes unacceptably small for very large objects. Indeed, in the limit $R_h \gg R_*$ the quantity directly constrained by stellar velocity dispersion data is the halo central density $\rho_0 = \Sigma_0/R_h$. Therefore, by moving along the χ^2 flat direction at increasingly larger radii in Figure 5, the halo mass increases as R_h^3 and eventually reaches values M_h that correspond to unacceptable friction times (15). This constraint is reported on Figs. 5, by cutting the region where friction times are unphysical.

In conclusion, the interplay between dynamical friction and velocity dispersion data allows us to determine an absolute upper bound on the halo size, and thus a lower bound on the DM mass. For Leo II, this results in a very weak constraint, $m \gtrsim 25$ eV.

4.2 Smallest Dwarf spheroidals: Willman I and Segue I

Let us apply the above strategies to the case of the Willman I and Segue I dwarf spheroidal galaxies (Willman et al. 2011; Simon et al. 2011) which are among the smallest galaxies for which line of sight velocities are available. Their stellar distributions are fitted by Plummer profiles with very small radii, given by $R_* = 25$ pc and $R_* = 29$ pc, respectively. We use the stellar velocity data to determine the averaged LOS velocity dispersion, equation (12), in three bins with extension comparable to the Plummer radii. The results obtained are reported in Figure 7 as a function of the projected distance from the galactic center. We compare these observational results with the theoretical predictions by repeating the procedure adopted for Leo II, i.e. we minimize $\chi^2(R_h, \Sigma_0, \beta)$ in the full range $-\infty < \beta \leq 1$ of the anisotropy nuisance parameter.

Our results are reported in figure 8, where we show the contours corresponding to 68% CL exclusion for $3-1 = 2$ dof for Willman I in the left frame and for Segue I in the right frame ($\chi^2 \equiv 2.3$).

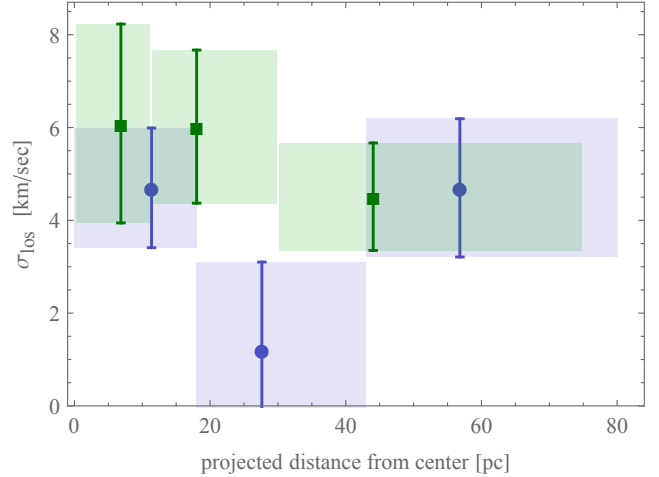


Figure 7. Line of sight velocity dispersion in Willman I (green squares) and Segue I (blue circles).

We note that no significant constraint on the halo radius is obtained for Willman I. Indeed, a good fit is achieved also for $R_h \ll R_*$ by allowing the anisotropy β to be increasingly negative. The fit worsens for large core radii but the χ^2 becomes flattish beyond $R_h \sim 300$ pc, not sufficiently large to give a significant exclusion of larger halo sizes. This is clearly due to the limited radial extension of the stellar data sample, ~ 75 pc. The best fit is obtained for $R_h \simeq 30$ pc, $\Sigma_0 = 473 M_\odot/\text{pc}^2$ and $\beta = -0.2$ and corresponds to $\chi^2 \simeq 0$, as it is expected by considering that we have only three bins and three free parameters.

Again, even if the DM radius is not constrained, the fits provide a useful determination of the central density of the system, that defines the flat direction in the plane (R_h, Σ_0) for $R_h \gg R_*$. Similarly to Leo II, by requiring that the dynamical friction decay time for Willman I is not unphysically small, we can exclude large core radii beyond $\sim \text{kpc}$ in the upper-right shaded region in 8 and obtain a robust lower bound on the DM mass, $m \gtrsim 80$ eV.

A similar analysis holds for Segue I, whose binned velocity dispersions are reported with blue circles in Figure 7. The three bins show that Segue I presents a different profile with respect to other dwarfs, with the velocity dispersion rising beyond ~ 40 pc. This behavior, that has already been noted in the literature as a possible evidence of a large DM halo (or an indication against its regularity/virialization) is consistent with the expectations from a scenario with $R_h \gg R_*$. Consistently, small radii $R_h \lesssim 40$ pc cannot be accommodated by the fit, even assuming a stellar anisotropy parameter $\beta \leq 0$. The best fit is obtained for $R_h \sim \text{few kpc}$ and no upper limits can be derived from Jeans analysis. Nevertheless, the central halo density is determined and the halo extension is limited again by the constraint on the dynamical friction time, as shown in Figure 8. The resulting lower bound on the DM mass is slightly better to that derived for Willman I, $m \gtrsim 100$ eV, mainly due to the fact that Segue I is closer to the galactic center.

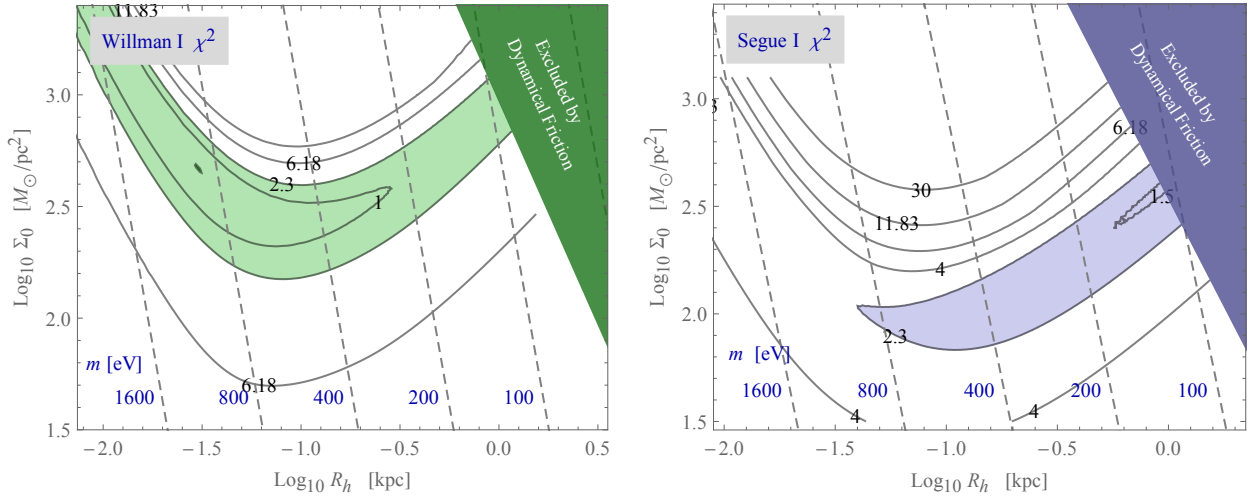


Figure 8. Contours of χ^2 , after minimizing on the free range of β . The left panel is for Willmann I, while the right panel refers to Segue I. The light shaded regions give the region of compatibility with data at 68% CL ($\chi^2 = 2.3$, 2 dof). Notice that no upper limit on the confidence interval on the radius can be placed for either galaxy.

4.3 Other Dwarfs

As a cross check, we note that the results presented above from the Jeans analysis are indeed compatible with the fits performed in the recent work from Hayashi et al. (2016) where the authors also consider the possibility of triaxial halos and arbitrary density profile slope at the center. While their analysis does not consider degenerate fermionic halos, their results confirm that for most dwarf galaxies the DM halo radius is quite poorly constrained, and halos of few kpc size appear to be allowed by data, even if this is most likely unphysical. For our purposes, as discussed above, what drives the bound on the DM mass is the interplay of the dynamical friction constraint with the central halo density ρ_0 , which is the quantity constrained by observations in the limit of large halo size. Because this central density is largely independent on the (outer) halo shape, we can take advantage of the results of Hayashi et al. (2016) to estimate the DM mass bound for all objects presented in that work. The bound is in fact driven by the central DM density and the distance of the dwarf satellite. As we see, by using the central fitted values of the densities, our result of Segue I and Leo II are confirmed, so that the results given in this work represent the most conservative bound around $m \gtrsim 100$ eV, with a possibly slightly stringent bound from the Triangulum II galaxy.

5 DISCUSSION AND CONCLUSIONS

In this work we have reassessed the lower bound on the mass of a fermionic dark matter candidate, independently from particular models of its production or history of its clustering. The quantum nature of such light fermionic candidate implies an upper bound on the phase space density in currently observed objects, and the knowledge of the density can be turned into a lower bound on the mass, *à la* Tremaine-Gunn. We have reconsidered the smallest Dwarf Spheroidal galaxies, that according to kinematical data are

Table 1. Estimated lower bound on the fermionic DM mass m from a number of dwarf spheroidal galaxies, adopting the central densities as determined in Hayashi et al. (2016).

DSph	$\text{Log } \rho_0$ [M_\odot/pc^3]	d_0 [kpc]	lower bound on m
Triangulum II	0.3	30	127 eV
Segue 1	-0.4	32	100 eV
Leo T	-0.6	417	26 eV
Reticulum II	-0.8	32	89 eV
Ursa Major I	-0.8	106	49 eV
Coma Berenices	-0.8	44	76 eV
Sculptor	-0.8	86	54 eV
Fornax	-1.1	147	38 eV
Ursa Major II	-1.2	32	80 eV
Leo I	-1.3	254	27 eV
Canes Venatici II	-1.4	151	34 eV
Hercules	-1.4	132	37 eV
Pisces II	-1.5	180	30 eV
Leo IV	-1.7	158	31 eV
Leo II	-1.7	233	25 eV
Draco II	-1.9	20	82 eV
Sextans	-2.	86	38 eV
Canes Venatici I	-2.2	224	22 eV
Carina	-2.2	106	33 eV
Bootes I	-2.4	66	39 eV
Leo V	-2.6	178	22 eV
Draco	-2.7	76	33 eV
Hydra II	-3.1	134	22 eV
Segue 2	-3.2	35	43 eV

believed to host the largest densities of dark matter, thus constituting the ideal candidates to set a lower bound on the DM mass m .

Such a bound must be set in the hypothesis that the DM halo of some of these objects is composed by a completely degenerate gas of fermions, whose density profile is defined by the Lane-Emden equation. We have performed a fit of the stellar velocity dispersion predicted by the gravitational potential generated by such DM halo, versus the observed

stellar dispersion velocity and density profile of the Willman I, Segue I and Leo II galaxies. In our analysis, differently from recent works on the subject, we have not assumed that luminous matter traces the DM distribution, thus we have considered the DM core radius and surface density as free parameters. Moreover, we have taken into account the effect of the unknown anisotropy of the stellar velocity dispersion and marginalized over it.

As we have shown, the nuisance due to the stellar velocity anisotropy β seriously hampers the possibility to efficiently constrain the DM halo parameters. In practice, one finds equally acceptable halos of very small sizes and negative β (where the total DM halo mass is determined) or very large sizes \sim few kpc and anisotropy near 1 (in which case the inner DM spatial density is determined). This latter scenario effectively corresponds to low phase-space densities, and thus no sensible lower bound on m can be given from stellar kinematical data alone. This situation is likely to persist even in the future, until a way to measure the velocity anisotropy in dwarfs spheroidals will be available (see e.g. Read & Steger (2017)) although this appears currently quite unconceivable.

New approaches have been proposed to circumvent the β -degeneracy in dwarf spheroidals in which sub-populations can be separated (Battaglia et al. 2008; Walker & Penarrubia 2011; Agnello & Evans 2012). These methods were applied to the Fornax galaxy in Amorisco et al. (2013) to exclude the NFW profile and constrain the DM distribution. The upper bound on Fornax core radius was used by Randall et al. (2017) to infer a lower limit $m > 70$ eV for the mass of a fermionic dark matter particle. Unfortunately, the likelihood distribution used to limit the core size in Amorisco et al. (2013) does not converge to zero for large core radii (see their Figure 4), as it is expected due to the fact that the stellar populations have limited extent. Therefore, while providing a robust lower bound for the core radius, even this approach cannot exclude few-kpc core radii at high confidence level.

Such multi-kpc halos are in any case unrealistic and a rationale to rule them out is provided Gerhard & Spiegel (1992) by the fact that very large halos of known density correspond to large total halo mass, which makes their time of orbital decay due to dynamical friction in the Galactic DM halo, formula (15), unphysically small. Therefore, dynamical friction can be used to effectively limit the halo size and the interplay with the quantum bound on phase-space density leads finally to a lower bound on the fermionic DM mass m .

As it turns out from the analysis that we described, at present the most restrictive bound stems from the study of the Willman I and Segue I galaxies. Our results are put together in Figure 1, where only the interplay between the fit to stellar data and the constraint from dynamical friction leads to a robust lower bound of $m \gtrsim 100$ eV. Thus, one is led to reopen the case for sub-keV fermionic DM, like sterile neutrinos of mass down to 100 eV.

For these two small dwarf galaxies driving the bound, the resulting DM halo can reach sizes of ~ 1 kpc, much larger than their stellar components. This does not mean that all the dwarf spheroidal galaxies shall have such enhanced halos;

this could likely hold only for these smallest objects that approach the fermionic degenerate regime.

As far as DM indirect detection is concerned, we note that the expected flux from DM annihilation (so called J -factor) is enhanced in the limiting case of the extended halo sizes considered here, compensating the naturally low flux characteristic of cored halos. At the same time, the dynamical friction upper bound on the halo sizes will slightly reduce the maximal expected J -factor in cored halos, with respect to the analysis of e.g. Hayashi et al. (2016).

Clearly, DM masses $m = 100$ eV are at odds with bounds derived from the effect of warm dark matter on structure formation (e.g. Lyman- α) that typically forbid masses below few keV, see e.g. Iršič et al. (2017), by limiting their free streaming length. Therefore, for this scenario to be realistic, the spectrum of such DM candidates should be much colder than usual (see e.g. Drewes et al. (2017)). This can be realized in models with production via decay as e.g. in Petraki & Kusenko (2008); Domcke & Urbano (2015), or for instance in models in which DM at decoupling is overabundant and then subject to dilution by decays of other species, along the lines of e.g. Bezrukov et al. (2010); Nemevsek et al. (2012).

More theoretically, in order to attain the fermionic degeneracy that we have tested, it is also necessary that either the maximum of the primordial phase-space density saturates the occupation limit (A5) as it happens e.g. in relativistic decoupling, or alternatively that DM is subject to some form of dissipation or interaction, so that the phase-space density might grow during collapse. Indeed, a very interesting (and outstanding) issue is that of which collapse mechanism and time scales could lead to degenerate fermionic halos. While the free energy and entropy budget have been shown to be favorable (Hertel et al. 1972; Bilic & Viollier 1997; Chavanis 2002), an assessment of the dynamics and relaxation times is still beyond reach, see Chavanis et al. (2015); Campa et al. (2009).

On the observational side, it is worth commenting that while the DSph galaxies are the smallest and most DM dominated astrophysical objects, with a number of new dwarfs being currently discovered by present surveys, the possibility of using other types of galaxies for setting a bound on m from degeneracy is also of interest. Recently, cored halo mass modelings of Disk Dwarf galaxies from the Little Things survey have been performed, see Karukes & Salucci (2017). Although the rotation curve decomposition is affected by uncertainty in the asymmetric drift gas contribution, due to their disk structure they are not subject to the dramatic anisotropy nuisance parameter of dwarf spheroidals and could potentially lead to a better bound on the DM mass m .

ACKNOWLEDGMENTS

We thank Neven Bilić, Kathy Karukes, Paolo Salucci and Piero Ullio for useful discussions. F.N. was partially supported by the H2020 CSA Twinning project No. 692194 “RBI-T-WINNING”. Results of this work were also presented in <https://indico.cern.ch/event/505065/contributions/2166456/>.

APPENDIX A: SELF-GRAVITATING FERMIONIC GAS

We briefly review in this appendix the analysis of the equilibrium distribution of a self-gravitating gas of neutral fermions. We describe first the limiting case of complete degeneration and then we recall the Thomas-Fermi treatment which allows to describe the transition to partially or non-degenerate case.

A0.0.1 Stability conditions for the DM halo. If we have large number of DM particles, we can assume they move in a spherically symmetric mean-field gravitational potential $\phi(r)$ which satisfies the Poisson's equation:

$$\begin{aligned} \frac{d\phi}{dr} &= \frac{GM}{r^2} \\ \frac{dM}{dr} &= 4\pi r^2 \rho, \end{aligned} \quad (\text{A1})$$

where $M(r)$ is the mass enclosed within the radius r , G is the Newton's constant and $\rho(r)$ is the matter density. For non relativistic particles, the density can be expressed as:

$$\rho = m \int dp 4\pi p^2 f(p), \quad (\text{A2})$$

where m is the particle mass and we assumed that DM distribution function $f(p)$ is isotropic. The dynamical stability of the system is expressed by the Jeans equation:

$$\frac{d}{dr}(\rho \sigma_{\text{DM}}^2) = -\rho \frac{d\phi}{dr}, \quad (\text{A3})$$

where the DM velocity dispersion σ_{DM}^2 is given by:

$$\sigma_{\text{DM}}^2 = \frac{1}{3} \frac{\int dp (p^4/m^2) f(p)}{\int dp p^2 f(p)} \quad (\text{A4})$$

If DM is composed by fermions, the distribution function $f(p)$ has an upper limit:

$$f(p) \leq \frac{g}{(2\pi\hbar)^3}, \quad (\text{A5})$$

where g represents the number of internal (spin) degrees of freedom. This automatically implies that a lower limit exists for the velocity dispersion

$$\sigma_{\text{DM}}^2 \geq \sigma_{\text{DM},\text{min}}^2 = \frac{1}{5} \left(\frac{6\pi^2 \hbar^3 \rho}{g m^4} \right)^{2/3} \quad (\text{A6})$$

of a fermionic system of fixed density.

A0.0.2 The strong degeneracy limit. In the strong degeneracy regime, the states with energy below the Fermi energy ε are fully occupied, i.e. the distribution function $f(p)$ has the form:

$$f(p) = \begin{cases} \frac{g}{(2\pi\hbar)^3} & p < p_{\text{F}} \\ 0 & p > p_{\text{F}} \end{cases} \quad (\text{A7})$$

where $p_{\text{F}} = \sqrt{2m\varepsilon}$ is the Fermi momentum. In this assumption, one obtains the expressions:

$$\begin{aligned} \rho &= K \varepsilon^{3/2} \\ \sigma_{\text{DM}}^2 &= K' \varepsilon, \end{aligned} \quad (\text{A8})$$

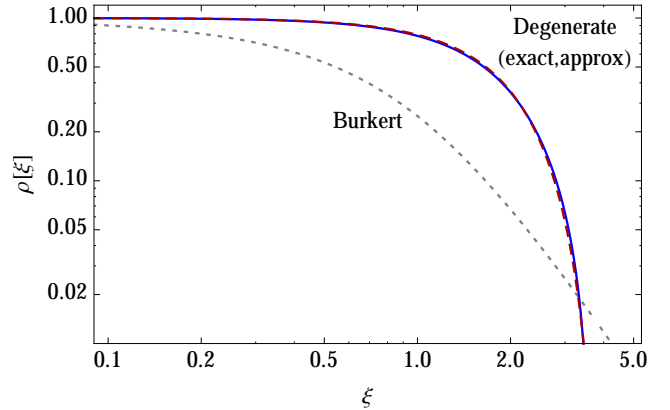


Figure A1. Density profiles for the DM halos. Solid: the solution of the Lane-Emden equation for degenerate fermions. Dashed: its approximation adopted in the text (A14). Dotted: the Burkert density profile for comparison.

where $K = \sqrt{2} g m^{5/2} / (3\pi^2 \hbar^3)$ and $K' = 2/(5m)$, so that Eqs. (A1,A3) can be recasted in the form

$$\frac{1}{r^2} \frac{d}{dr} \left[r^2 \frac{d\varepsilon(r)}{dr} \right] = -4\pi G m K \varepsilon(r)^{3/2}. \quad (\text{A9})$$

This equation has to be integrated with the condition $d\varepsilon(0)/dr = 0$ ensuring that the gravitational acceleration is zero at the center. By defining

$$\xi \equiv r/\tilde{r}, \quad (\text{A10})$$

where the scale radius \tilde{r} is given by

$$\tilde{r} \equiv \frac{1}{\sqrt{4\pi G m K \varepsilon_0^{1/2}}} = \frac{1}{\sqrt{4\pi G m K^{2/3} \rho_0^{1/3}}}, \quad (\text{A11})$$

and by using the function $\theta(\xi)$ defined as

$$\theta(\xi) \equiv \frac{\varepsilon(\xi)}{\varepsilon_0} = \left[\frac{\rho(\xi)}{\rho_0} \right]^{2/3}, \quad (\text{A12})$$

where ε_0 (ρ_0) is the central value of the Fermi energy (density), equation (A9) can be rewritten in the form

$$\frac{1}{\xi^2} \frac{d}{d\xi} \left[\xi^2 \frac{d\theta(\xi)}{d\xi} \right] = -\theta(\xi)^{3/2}, \quad (\text{A13})$$

which is the well-know Lane-Emden equation.

Eqs. (A12) and (A13) show that the profiles of degenerate Fermionic DM halos are universal and depend only on the assumed central density ρ_0 and DM particle mass m . The mass distribution crucially differs from the usually adopted cusped or cored profiles. A sharp transition exists from an internal core with quite uniform density to an external region devoid of DM. For our purposes, the density profile of degenerate fermionic DM halos can be well approximated by

$$\rho(\xi) = \rho_0 \cos^3 \left[\frac{\pi}{8} \xi \right] \quad (\text{A14})$$

for $0 \leq \xi \leq 3.65$, and $\rho(\xi) = 0$ elsewhere, see Figure A1.

We define the halo radius by the condition $\rho(\xi_h) = \rho_0/4$ that gives $\xi_h = 2.26$ corresponding to:

$$\begin{aligned} R_h &\equiv \xi_h \tilde{r} = & (A15) \\ &= 2.26 \left(\frac{9\pi}{27} \right)^{\frac{1}{6}} \frac{\hbar}{G^{1/2}} g^{-\frac{1}{3}} m^{-\frac{4}{3}} \rho_0^{-\frac{1}{6}} = \\ &= 42.4 \text{ pc} \left(\frac{g}{2} \right)^{-1/3} \left(\frac{m}{1 \text{ keV}} \right)^{-4/3} \left(\frac{\rho_0}{\text{M}_\odot/\text{pc}^3} \right)^{-1/6}. \end{aligned}$$

By using the above expression, we rewrite equation (A14) in the form:

$$\rho(r) = \rho_0 \cos^3 \left[\frac{25}{88} \pi \frac{r}{R_h} \right], \quad (A16)$$

where we used the approximate equality $\xi_h/8 \simeq 25/88$.

A0.0.3 The Thomas-Fermi model for fermionic DM. A self consistent description of isothermal fermionic DM halos with an arbitrary level of degeneration can be obtained by using a Thomas-Fermi approach, see Bilic et al. (2001); de Vega et al. (2014). One assumes that DM particles follow a Fermi-Dirac distribution

$$f_{\text{FD}}(p; T, \mu) = \frac{g}{(2\pi\hbar)^3} \frac{1}{\exp[(E - \mu)/T] + 1}, \quad (A17)$$

where $E = p^2/(2m)$ is the single-particle kinetic energy, T is the temperature expressed in terms of energy and μ is the chemical potential. In the above, the density can be expressed as:

$$\rho = \frac{g(2T)^{3/2} m^{5/2}}{6\pi^2 \hbar^3} I_2(\nu), \quad (A18)$$

where

$$I_2(\nu) \equiv 3 \int_0^\infty dy \frac{y^2}{\exp(y^2 - \nu) + 1} \quad (A19)$$

and $\nu \equiv \mu/T$ is a degeneracy parameter.

If one assumes a constant temperature, $T(r) \equiv \tilde{T}$, and that the chemical potential at each given radius includes the gravitational potential $\phi(r)$ as

$$\mu(r) = \tilde{\mu} - m\phi(r) \quad (A20)$$

where $\tilde{\mu}$ is a constant, then the Jeans equation (A3) is automatically fulfilled and Eqs. (A1), (A2) can be recast in the form

$$\frac{1}{r^2} \frac{d}{dr} \left[r^2 \frac{d\mu(r)}{dr} \right] = -4\pi G m \rho(r), \quad (A21)$$

again to be integrated with the condition $d\mu(0)/dr = 0$ for zero gravitational acceleration at the galaxy center.

A0.0.4 The non degenerate case. The Thomas-Fermi approach just described has the advantage of automatically implementing the upper limit (A5) imposed by the Pauli exclusion principle; it can thus describe the transition between classical and degenerate structures, in a continuous way. By using this approach, one is able to see that when R_h is 2-3 times larger than the minimal value in equation (A15) the fermionic nature of DM particles can be neglected, i.e. the resulting structures are essentially indistinguishable from cored isothermal halos obtained by assuming

Maxwell-Boltzmann statics and arbitrary values of the particle mass m .

This approach does not allow, however, to unambiguously predict the halo properties in the non degenerate case. Indeed, in the classical regime (i.e. for $\nu \ll 1$) one has $I_2(\nu) \simeq \exp(\nu)$, differently from the strongly degenerate case in which $I_2(\nu) \simeq \nu^{3/2}$. Thus, the r.h.s. of equation (A21) depends both on the temperature and the chemical potential. One obtains then a family of solutions depending on these two free parameters: the temperature \tilde{T} and the assumed chemical potential μ_0 (or, equivalently, the assumed density ρ_0) at the center of the system. Moreover, a temperature profile, here constant, had to be assumed in the Thomas-Fermi approach in order to solve equation (A3). In a more realistic scenario, in which the temperature may vary along the galactic structure, \tilde{T} could be regarded as the central temperature; the predictions obtained in the degenerate or semi-degenerate regimes are thus valid in the central core where temperature variations can be neglected, while the properties of the external region depend on the radial temperature profile. As it is natural to expect, basing on sole theoretical grounds it is thus impossible to predict the mass distribution in regions of non degeneration.

For this reason in the text, where we refer to non-degenerate halos, we model them by using the observationally supported Burkert profile:

$$\rho_{\text{Bur}}(r) = \frac{\rho_0}{(1+x)(1+x^2)}, \quad x = r/R_h. \quad (A22)$$

In using this profile, we require that the central density ρ_0 and core radius R_h are consistent with the assumption of non degenerate structure composed by fermions with mass m and g spin degrees of freedom, i.e. for each assumed value of ρ_0 , the halo radius R_h is required to be a factor ~ 2 larger than the degenerate limit expressed by equation (A15).

REFERENCES

- Agnello A., Evans N. W., 2012, *Astrophys. J.*, 754, L39
 Amorisco N. C., Agnello A., Evans N. W., 2013, *Mon. Not. Roy. Astron. Soc.*, 429, L89
 Avila-Reese V., Colin P., Valenzuela O., D'Onghia E., Firmani C., 2001, *Astrophys. J.*, 559, 516
 Battaglia G., Helmi A., Tolstoy E., Irwin M., Hill V., Jablonka P., 2008, *Astrophys. J.*, 681, L13
 Bezrukov F., Hettmansperger H., Lindner M., 2010, *Phys. Rev.*, D81, 085032
 Bilic N., Viollier R. D., 1997, *Phys. Lett.*, B408, 75
 Bilic N., Tupper G. B., Viollier R. D., 2001, preprint ([arXiv:astro-ph/0111366](https://arxiv.org/abs/astro-ph/0111366))
 Binney J., Tremaine S., 2008, *Galactic Dynamics*, 2nd edition. Princeton University Press
 Bode P., Ostriker J. P., Turok N., 2001, *Astrophys. J.*, 556, 93
 Boyarsky A., Ruchayskiy O., Iakubovskiy D., 2009, *JCAP*, 0903, 005
 Campa A., Dauxois T., Ruffo S., 2009, *Phys. Rept.*, 480, 57
 Chavanis P.-H., 2002, *Phys. Rev.*, E65, 056123
 Chavanis P.-H., Lemou M., Méhats F., 2015, *Phys. Rev.*, D91, 063531
 Colin P., Avila-Reese V., Valenzuela O., 2000, *Astrophys. J.*, 542, 622

- Dalcanton J. J., Hogan C. J., 2001, *Astrophys. J.*, 561, 35
- Domcke V., Urbano A., 2015, *JCAP*, 1501, 002
- Donato F., et al., 2009, *Mon. Not. Roy. Astron. Soc.*, 397, 1169
- Drewes M., et al., 2017, *JCAP*, 1701, 025
- Flores R. A., Primack J. R., 1994, *Astrophys. J.*, 427, L1
- Gerhard O. E., Spergel D. N., 1992, *The Astrophysical Journal Letters*, 389, L9
- Governato F., et al., 2010, *Nature*, 463, 203
- Governato F., et al., 2012, *Mon. Not. Roy. Astron. Soc.*, 422, 1231
- Hayashi K., Ichikawa K., Matsumoto S., Ibe M., Ishigaki M. N., Sugai H., 2016, *Mon. Not. Roy. Astron. Soc.*, 461, 2914
- Hertel P., Narnhofer H., Thirring W. E., 1972, *Commun. Math. Phys.*, 28, 159
- Iršič V., et al., 2017
- Just A., Khan F. M., Berczik P., Ernst A., Spurzem R., 2011, *Mon. Not. Roy. Astron. Soc.*, 411, 653
- Karukes E. V., Salucci P., 2017, *Mon. Not. Roy. Astron. Soc.*, 465, 4703
- Klypin A. A., Kravtsov A. V., Valenzuela O., Prada F., 1999, *Astrophys. J.*, 522, 82
- Moore B., 1994, *Nature*, 370, 629
- Moore B., Quinn T. R., Governato F., Stadel J., Lake G., 1999a, *Mon. Not. Roy. Astron. Soc.*, 310, 1147
- Moore B., Ghigna S., Governato F., Lake G., Quinn T. R., Stadel J., Tozzi P., 1999b, *Astrophys. J.*, 524, L19
- Navarro J. F., Eke V. R., Frenk C. S., 1996a, *Mon. Not. Roy. Astron. Soc.*, 283, L72
- Navarro J. F., Frenk C. S., White S. D. M., 1996b, *Astrophys. J.*, 462, 563
- Navarro J. F., Frenk C. S., White S. D. M., 1997, *Astrophys. J.*, 490, 493
- Nemevsek M., Senjanovic G., Zhang Y., 2012, *JCAP*, 1207, 006
- Nesti F., Salucci P., 2013, *JCAP*, 1307, 016
- Petraki K., Kusenko A., 2008, *Phys. Rev.*, D77, 065014
- Pontzen A., Governato F., 2012, *Mon. Not. Roy. Astron. Soc.*, 421, 3464
- Randall L., Scholtz J., Unwin J., 2017, *Mon. Not. Roy. Astron. Soc.*, 467, 1515
- Read J. I., Steger P., 2017, preprint, ([arXiv:1701.04833](https://arxiv.org/abs/1701.04833))
- Read J. I., Goerdt T., Moore B., Pontzen A. P., Stadel J., Lake G., 2006, *Mon. Not. Roy. Astron. Soc.*, 373, 1451
- Salucci P., Burkert A., 2000, *Astrophys. J.*, 537, L9
- Salucci P., Wilkinson M. I., Walker M. G., Gilmore G. F., Grebel E. K., Koch A., Martins C. F., Wyse R. F. G., 2012, *Mon. Not. Roy. Astron. Soc.*, 420, 2034
- Simon J. D., et al., 2011, *Astrophys. J.*, 733, 46
- Tremaine S., Gunn J. E., 1979, *Phys. Rev. Lett.*, 42, 407
- Ullio P., Valli M., 2016, *JCAP*, 1607, 025
- Walker M., 2013, Dark Matter in the Galactic Dwarf Spheroidal Satellites. p. 1039, doi:10.1007/978-94-007-5612-0_20
- Walker M. G., Penarrubia J., 2011, *Astrophys. J.*, 742, 20
- Walker M. G., Mateo M., Olszewski E. W., Gnedin O. Y., Wang X., Sen B., Woodroffe M., 2007, *Astrophys. J.*, 667, L53
- Weinberg D. H., Bullock J. S., Governato F., Kuzio de Naray R., Peter A. H. G., 2014, *Proc. Nat. Acad. Sci.*, 112, 12249
- Willman B., Geha M., Strader J., Strigari L. E., Simon J. D., Kirby E., Warres A., 2011, *Astron. J.*, 142, 128
- Wolf J., Martinez G. D., Bullock J. S., Kaplinghat M., Geha M., Munoz R. R., Simon J. D., Avedo F. F., 2010, *Mon. Not. Roy. Astron. Soc.*, 406, 1220
- de Vega H. J., Salucci P., Sanchez N. G., 2014, *Mon. Not. Roy. Astron. Soc.*, 442, 2717

This paper has been typeset from a $\text{\TeX}/\text{\LaTeX}$ file prepared by the author.